



Measurements on the effect of steps on the transition of laminar boundary layers

Alexander Heintz^{1,2} · Peter Scholz¹

Received: 3 November 2022 / Revised: 21 December 2022 / Accepted: 2 March 2023
© The Author(s) 2023

Abstract

The effects of steps on the transition of laminar boundary layers were measured on a flat plate for low Reynolds numbers with critical and subcritical step heights. The transition position was measured by determining the intermittency distribution in streamwise direction, including the characteristic length of the transitional region. The results are compared with formulations of a critical step Reynolds number Re_h , i.e., the step height that will instantly trigger transition at the step position, and—for subcritical step heights—with ΔN -formulations from the literature. For backward-facing steps, the concept of a step Reynolds number can be used to distinguish between subcritical and critical step heights, whereas for forward-facing steps there seems not to be one unique Re_h . Furthermore, for subcritical backward-facing steps the concept of a ΔN -approximation gives a reasonable description of the experimental observations. Again in contrast, for forward-facing steps a ΔN -approach scattered a lot and no clear dependency was found between the reduction in the critical N-factor of transition and the relative step height.

1 Introduction

Increasing laminar flow regions on aircraft surfaces to decrease skin friction is a well-known and established method covering many aspects, such as natural laminar flow (NLF), laminar flow control (LFC) or hybrid approaches. However, laminar boundary layers are very sensitive to surface imperfections, particularly backward- and forward-facing steps. In many practical considerations, such as the design of aircraft or dedicated wind tunnel experiments, it is important to estimate the effect of such steps on the transition process.

For tube flows, Schiller (1932) first hypothesized that the critical Reynolds number, formed with the step height, is a good estimate of a critical roughness. He already recognized a reduction in the laminar region for uncritical step heights and suggested an influence on the stability. In the 1940s Tani, Hama and Mituisi followed this idea and used Taylor's identifiers to show how this Reynolds numbers might relate to the magnitude of the imperfections, see Tani and Hama (1953). Fage (1943) was then the first to show that the transition position is repeatably related to the step height h .

The two most basic versions of surface imperfections are forward- and backward-facing steps, FFS an BFS, respectively. For these types, Nenni and Gluyas (1966) developed a criterion to estimate whether a step induces transition to turbulence immediately, i.e., triggers bypass transition, using the Reynolds number based on the step height:

$$Re_h = \frac{u_e \cdot h}{\nu}, \quad (1)$$

where u_e is the boundary layer edge velocity, h is the height of the step and ν is kinematic viscosity.

The critical step Reynolds numbers are

$$Re_{h,BFS} = 900 \quad (2)$$

for backward-facing and

Alexander Heintz and Peter Scholz have contributed equally to this work.

✉ Alexander Heintz
alexander.heintz@dlr.de

Peter Scholz
p.scholz@tu-braunschweig.de

¹ Institute of Fluid Mechanics, Technische Universität Braunschweig, Hermann-Blenk-Str. 37, 38108 Braunschweig, Lower Saxony, Germany

² Present Address: Institute of Aerodynamics and Flow Technology, German Aerospace Center, Bunsenstr. 10, 37073 Göttingen, Lower Saxony, Germany

$$\text{Re}_{h,\text{FFS}} = 1800 \quad (3)$$

for forward-facing steps. These values were determined empirically based on data from flight experiments with the X-21 test vehicle.

Note that for boundary layers with pressure gradients a slightly different step Reynolds number, e.g., used by Smith and Clutter (1959), Eppler (1990) and others, may be useful, which is

$$\text{Re}_h = \frac{u_h \cdot h}{\nu} \quad (4)$$

where u_h is the velocity in the boundary layer at the height h . For zero pressure gradient cases with constant Blasius profile, the two different definitions of Re_h have a fixed relation to each other. For favorable or adverse pressure gradient boundary layers, the refined version with u_h may be more suitable to respect the influence of the boundary layer velocity profile. Since herein we will only cover cases with constant velocity profiles near zero pressure gradient, both definitions should follow the same trends. We will therefore use the original formulation with u_c from Nenni and Gluyas (1966).

The critical Reynolds number is a simple binary criterium, but already Schiller (1932) has recognized that non-critical disturbances still have an influence on the transition position. This is due to a destabilizing influence on the modal disturbances, i.e., the Tollmien–Schlichting waves, that evolve in a laminar boundary layer. The most widely used method to predict the development of these disturbances and the transition to turbulence is linear stability theory and the e^n method, van Ingen (1956) and Smith and Gamberoni (1956), where the local amplitude of the disturbances is finally expressed as an N-factor. Consequently, Wie and Malik (1998) proposed to find a relationship as a difference between the N-factor N_0 for the case without step and the N-factor N_{St} for the case with step. If the step acts as an amplification of existing Tollmien–Schlichting waves, this can be expressed by a ΔN , which should somehow correlate with the step height in the subcritical range.

Wang and Gaster (2005) estimated the development of ΔN with the step height normalized with the displacement thickness h/δ^* . According to the authors, the resulting data should “provide a useful guide” to estimate the influence of backward- and forward-facing steps. Crouch et al. (2006) and Perraud et al. (2014) suggested linear correlations between the length scale of the boundary layer and the value of ΔN :

$$\text{Perraud et al., BFS} : \Delta N = 1.515 \frac{h}{\theta} - 0.44 \quad (5)$$

$$\text{Crouch et al., BFS} : \Delta N = 4.4 \frac{h}{\delta^*} \quad (6)$$

$$\text{Crouch et al., FFS} : \Delta N = 1.6 \frac{h}{\delta^*} \quad (7)$$

These estimations were found by linear regressions of measured data. Differences between (5) and (6) are primarily for very small or very large Reynolds numbers. The ΔN -values from Wie and Malik (1998) differ especially for small h/δ^* , since they are not linear in this region. Finally, the correlations from Hildebrand et al. (2020) are designed to give a better fit, while still including the data from Crouch et al. (2006). Their version is:

$$\Delta N = \begin{cases} 2.47(h/\delta^*)^2 + 0.62(h/\delta^*), & \text{if } h/\delta^* < 0.38 \\ 3.0(h/\delta^*) - 0.55, & \text{if } h/\delta^* \geq 0.38. \end{cases} \quad (8)$$

It seems that particularly for small disturbances, and small ΔN , respectively, still data are required to verify whether the correlations of $\Delta N(h)$ really have universal character. Therefore, in the present paper, we contribute additional experimental data for subcritical and critical steps, both BFS and FFS, at low Reynolds numbers.

The results will be analyzed in two steps: First, the Reynolds number Re_h will be used to differentiate between subcritical and critical steps and the validity of the Re_h criteria (2) and (3) will be assessed. Then, the subcritical data will be compared with the empirical ΔN -formulations (5) to (8).

2 Methodology

2.1 Experimental setup

The experiments were done in the low-speed Eiffel-type wind tunnel LNB (*Leiser Niedergeschwindigkeitswindkanal Braunschweig*) in the Institute of Fluid Mechanics at Technische Universität Braunschweig. The tunnel has a closed, rectangular test section with a length of 1500 mm, a width of 400 mm and a height of 600 mm. The flow is conditioned in the settling chamber with a straightener and two screens and then passes through a nozzle with a contraction of 1:15, which is based on the design rules for minimum length wind tunnel nozzles from Börger (1975). The freestream turbulence level varies between 0.2 and 0.075% and will be discussed later in Sect. 2.3. For the measurements discussed herein, the tunnel was operated with freestream velocities between 4 and 19.5 m/s.

A flat plate element with a chord length of $c = 1400$ mm spanning the full width of 400 mm was mounted in the

centerline of the tunnel. In streamwise direction, the flat plate consists of four elements: the leading edge ($0 < x/c < 0.12$), flat element #1 ($0.12 < x/c < 0.42$), flat element #2 ($0.42 < x/c < 0.72$) and the trailing edge ($0.72 < x/c < 1.0$), which tapers to realize a small trailing edge thickness.

The leading edge contour is a custom design to avoid an excessive suction peak and the associated adverse pressure gradient in the leading edge region. The approach is similar to, e.g., Grappadelli et al. (2021). Then comes a fixed, plain flat plate region. At the position $x/c = 0.42$ between the two flat elements, a step with freely adjustable height is integrated. To generate the step, the second element of the plate, which in itself is also plain and flat, is hinged with a flexure bearing near the trailing edge. With this arrangement, effectively a variation of the step height creates a small pressure gradient on the second part of the flat plate. However, due to the length of the second element this pressure gradient is literally negligible. In any case, as will be discussed in Sect. 2.3, the measured pressure distribution was used for the stability calculations. Hence, even if this effect may be of any relevant magnitude, it will be accounted for in the analysis process.

The steps are only realized on the one side of the otherwise fully symmetrical flat plate. Measurements were taken for the step heights 0.5 mm, 1 mm, 1.5 mm and 2 mm for backward- and forward-facing steps and for forward-facing steps also with 3 mm. The steps are set with two spring-loaded micrometer screws, which are built into the flat plate element and can be accessed from the bottom side. The step can be set with an accuracy of around $\sigma_h \approx 0.05$ mm, which is the accuracy of the micrometer screws. For selected cases, the step height was also cross-checked with a precision caliper and was always within the specifications of the micrometer screws.

Due to the limited tunnel velocities, a flat plate with zero pressure gradient requires a rather long distance to transition to turbulence. The length of the plate is, however, limited by the test section length. To cope with this problem, the bottom and top walls of the wind tunnel are equipped with adjustable plates, as shown in Fig. 1, forming a diffuser that can be adjusted with micrometer screws. For all data—with one exception—that will be presented herein, the diffuser plates were set to an opening half-angle of $\beta = 1.2^\circ$. This setting was found iteratively in the test itself, by varying the wind tunnel velocity and the diffuser angle, until the natural transition on the plate near maximum tunnel velocity is near the position of the step, which allows to gather data over the full velocity range of the tunnel. As a consequence, however, the flow over the flat plate is not strictly a Blasius-type boundary layer, but features a weak adverse pressure gradient. Pressure distribution and boundary layer development will be shown in Sect. 2.3.

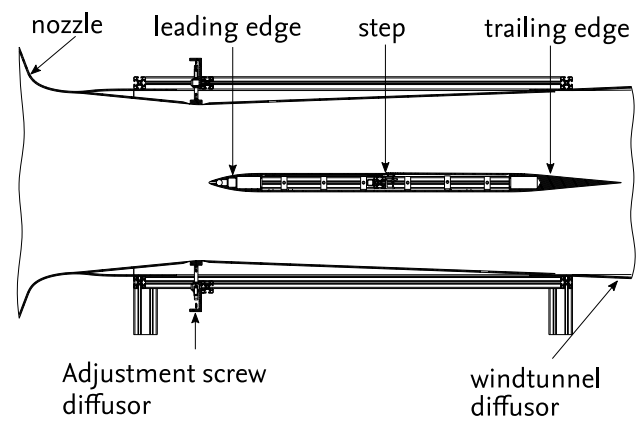


Fig. 1 Overview over the experiment

The one exception mentioned above is the calibration of N_{crit} : With the standard opening angle of the diffuser of $\beta = 1.2^\circ$, the transition reaches the trailing edge region of the flat plate at a wind tunnel velocity of approximately $u_\infty = 13$ m/s. Hence, N_{crit} cannot be found from a direct measurement above this velocity. Therefore, one dataset (to be shown in Fig. 10) was acquired with a smaller opening angle of $\beta = 0.8^\circ$, which reduces the adverse pressure gradient, makes the boundary layer slightly more stable and, thus, allows calibration of N_{crit} at larger velocities.

2.2 Measurement methods

Several pressure taps are fitted into the flat plate and the wind tunnel top and bottom wall to measure static pressure distributions. The taps are connected to a DTC Initium pressure scanner system. The nominal accuracy of the pressure scanners is $\sigma_p \approx 3.4$ Pa. On the flat plate, the pressure taps are integrated not along the centerline, but off-center, so as to avoid that any turbulence wedges/spots, which may be generated due to the taps, can interfere with the flow probes.

To measure freestream turbulence, a commercial hotwire system Dantec Streamline Pro with a Dantec 55P11 miniature wire probe was used. To measure boundary layer velocity profiles, the same wire probe was mounted on a small mechanical traversing system. The hotwire signal output was calibrated w.r.t. velocity in the same wind tunnel. For the sake of brevity, since the hotwire data will not be the core of the data presented herein, we will not go into detail regarding the bridge balancing and hotwire calibration procedures. All setup and calibration is done according to the operation manuals of this commercial system.

To accurately measure the transition position, the intermittency curve in the transitional region was measured using a staggered row of six wall-mounted Pitot tubes, also known as Preston probes, as shown in Fig. 2. Each probe is connected to a condenser microphone and the resulting voltage



Fig. 2 The aft end of the flat plate setup mounted in the wind tunnel showing the staggered row of Preston probes

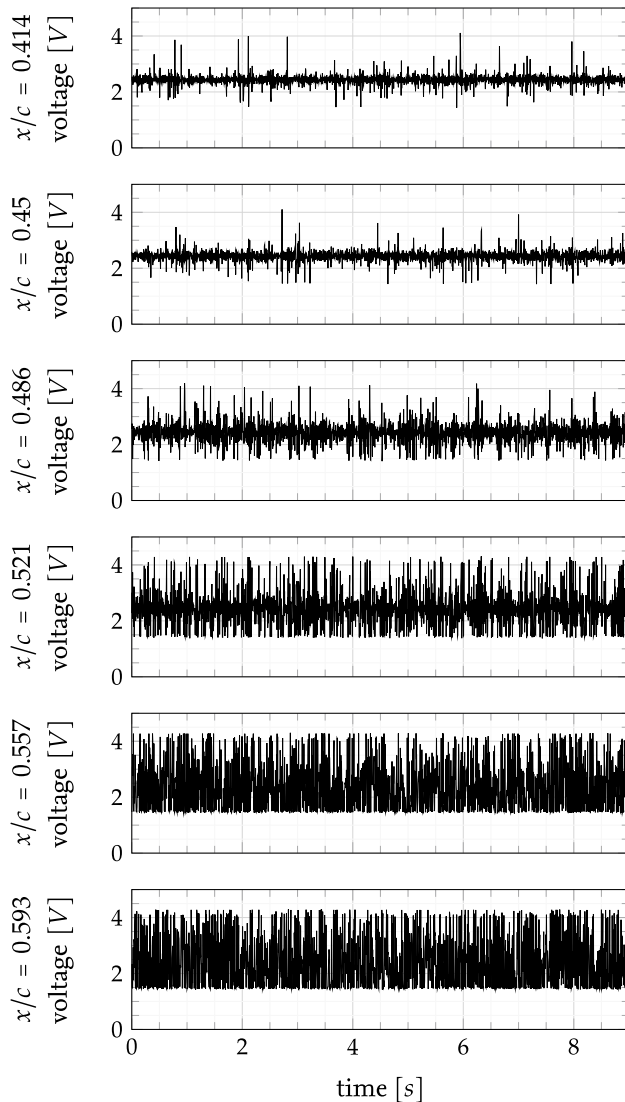


Fig. 3 Raw signal of dynamic pressure fluctuations (not calibrated) at different streamwise positions

is the raw signal that will be used to post-process the intermittency distribution $\gamma(x)$.

Figure 3 shows the raw signal for one of the test cases as an example. Increasing intermittency with chord length is clearly visible. In contrast to, e.g., the signal from a surface hotfilm, the microphone signals do not carry any reliable information about the shear stress itself, but only on the fluctuating components. Therefore, a post-processing is essential and the core steps will briefly be outlined in the following.

The threshold to switch between laminar and turbulent times is applied to the simple moving average of the function $(|E| - \min(|E|))$, where E is the raw voltage.

To define the threshold itself, the microphone signal of a fully turbulent flow some distance behind a transition tape with a sufficient thickness was measured over the entire freestream velocity range. The mean value of these signals gave an almost linear function of $\overline{|E_{\text{turb}}|}(u_\infty)$ and the magnitude of this average was very clearly larger than the signal of a laminar flow. Therefore, half of the turbulent average, i.e., $0.5 \cdot \overline{|E_{\text{turb}}|}(u_\infty)$, was used as the threshold value.

The timescale of the simple moving average filter was chosen to be 6 ms. Figure 4 shows the raw signal and the resulting turbulence detector for one case as an example.

The influence of the two parameters involved in this process, i.e., the threshold factor and the moving average timescale, was studied by measurements without steps, where the freestream velocity was varied in fine steps, such that the full intermittency curve is resolved in many different positions, Fig. 5. With these raw data, the resulting intermittency curves for several different combinations of the two parameters were compared with the theoretical distribution from the theory of Narasimha (1957). Figure 5 shows the final outcome of this study, where the measured data are an adequate representation of the expected outcome.

We note that the choice of both parameters was suitably robust. Changing the threshold factor in a certain range does not substantially change the appearance of the intermittency curve shown in Fig. 5. A too low threshold factor is quickly evident by the fact that the measured data would not decay to zero for the laminar part and a too high threshold factor

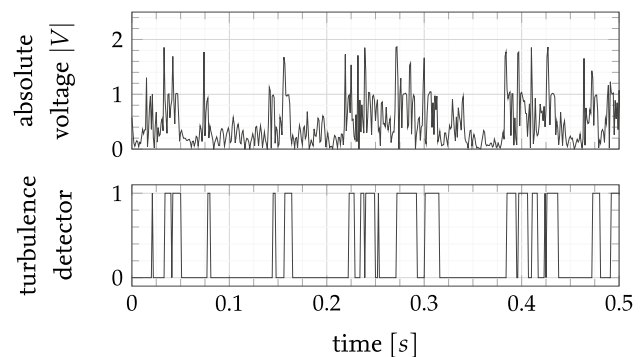


Fig. 4 Turbulence detection for a signal with a dynamic averaging interval of 6 ms

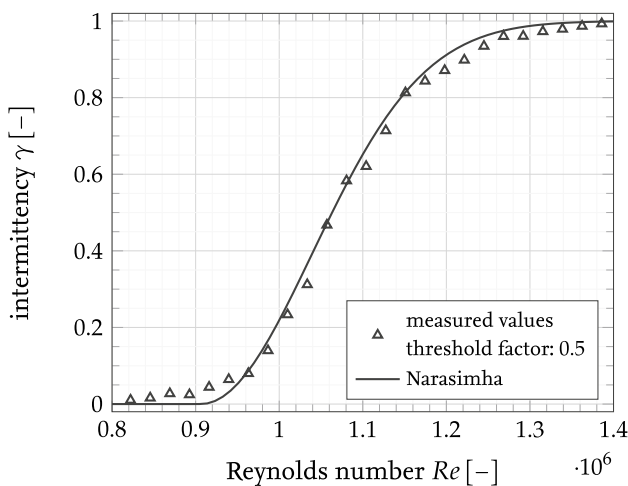


Fig. 5 Comparison of the measured intermittency and the theory of Narasimha (1957) over the velocity, given by the Reynolds number, at the point $x/c = 0.486$

would not give $\gamma = 1$ in the turbulent region, respectively. The same is true for an obviously wrong choice of the moving average timescale.

While for this calibration study a fine distribution of the intermittency curve along chord (or with Re) is possible, for the production measurements with steps much lesser support points along x will be available. To fit a continuous development of the intermittency, we assume the relation of Emmons (1951) and Narasimha (1957):

$$\gamma = 1 - e^{[-0.412(\xi+1.3)^2]}, \tag{9}$$

where ξ is the dimensionless chordwise distance, which in turn is defined as:

$$\xi = \frac{x - \bar{x}}{\lambda}. \tag{10}$$

Here, λ is the characteristic length of the transitional region, which is defined as the distance between the positions $x(\gamma = 0.25)$ and $x(\gamma = 0.75)$ and \bar{x} is the start position of the transitional region.

This formulation finally has two free parameters: λ and \bar{x} , which were determined by a least square fit to the measured intermittency values. Although \bar{x} is formally the “initiation point of transition,” i.e., the first position along x where turbulent spots may appear, herein we will consistently use a different definition of the point of transition. The reason is that in the majority of other experiments (particularly experiments with infrared imaging) \bar{x} can practically not be determined. Therefore, for all subsequent analyses, we consistently define “the transition position” to be the chordwise location, where intermittency has reached a notable value. Specifically we define:

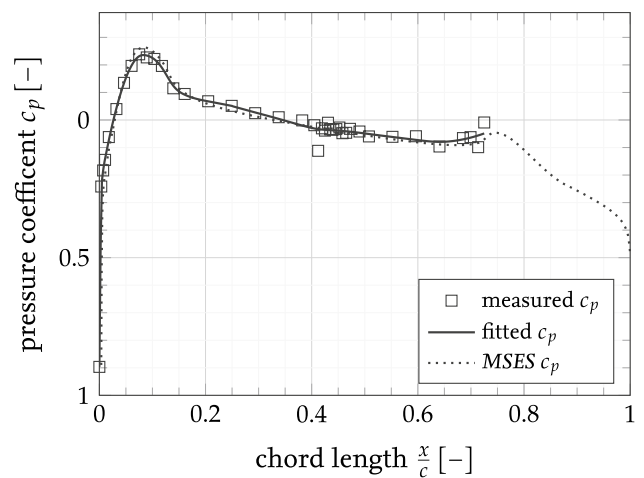


Fig. 6 Example of a measured pressure distribution over the top side

$$x_{tr.} := x(\gamma = 0.2). \tag{11}$$

Note that the theory of Emmons (1951) and Narasimha (1957) in Eq. (9) is based on two assumptions: for one on the findings from Schubauer and Klebanoff (1955) that the diffusion of turbulence creates a true cone or, in other words, straight propagation lines of turbulent spots and on the other hand, the theory of concentrated breakdown. Concentrated breakdown means that the source function, i.e., the probability distribution of the spot nucleation, is a Dirac’s delta function. It may well be debatable whether these assumptions are valid—both, for transition behind a step, or even in general. For all of our cases, as will be shown in later sections, the function (9) fitted well to the support points and gave a consistent and repeatable way to define the transition position. Also the transition length λ showed repeatable and physically comprehensible behavior. Therefore, we assume that these two conditions are fulfilled good enough such that Eq. (9) is applicable herein.

2.3 Stability analysis and validation

For the boundary layer and stability analysis, the boundary layer solver COCO, Schrauf (1998), and the linear local stability analysis method LILO, Schrauf (2006), are used. This chain (the combination often called COCOLILO) is very widespread in German aeronautical research, so a more detailed description of these two methods will not be given here. Data can be found, e.g., in Krumbein et al. (2009) and the references therein.

For the boundary layer solver, the measured pressure on the flat plate was used as an input. To increase the spatial resolution and to avoid non-physical data from the pressure sensor noise, a smoothing spline is fitted to the experimental data. Figure 6 shows the result of this process. The same

figure also shows a simulation of the setup with the Euler method *MSES*, which agrees very well with the experimental and the fitted data, which gives confidence that the geometry itself and the smoothing is valid and consistent.

The measured pressure distribution was almost literally independent from the wind tunnel velocity. Therefore, the stability simulations were effectively done based on one and the same pressure distribution for all tunnel velocities.

To evaluate and verify the quality of the boundary layer solution, velocity profiles were measured with a traversing hotwire probe. The comparison between the measured velocity profile and the accompanying prediction from the boundary layer method is shown in Fig. 7. Generally, the data agree very well. We can only find a small deviation near to the surface, which results from the heat radiated from the sensor that gets reflected on the surface.

One resulting N-factor diagram for critical frequencies is shown in Fig. 8. Typical for flows with a constant, weak adverse pressure gradient at low Re is a rather slow gradient of the envelope along x/c , which makes this type of flows sensitive to the different disturbances of the steps.

The core of the e^N method is to compare this amplitude factor N with a critical N-factor N_{crit} , which indicates the transition start. N_{crit} generally depends on the flow quality of the wind tunnel. Herein, two methods to determine N_{crit} were tested and compared against each other: First, a direct measurement of N_{crit} by measuring x_{tr} using the methods described above, but also a measurement of the turbulence level Tu of the wind tunnel and then using the correlations of Mack (1975) or van Ingen (2008).

For the latter, it is worthwhile to note that these two (empirical) correlations differ in detail: The one from Mack (1975) only gives one single N_{crit} , whereas (van Ingen 2008)

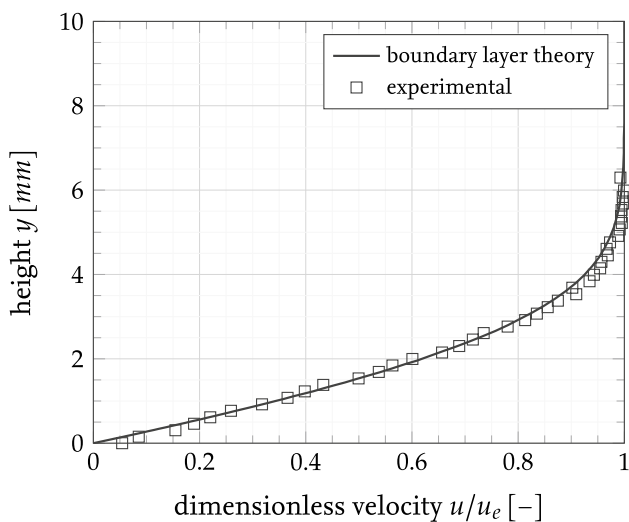


Fig. 7 Velocity profile from a hotwire measurement and based on the boundary layer method COCO, $x/c = 0.41$ at $Re = 5.5 \cdot 10^5$

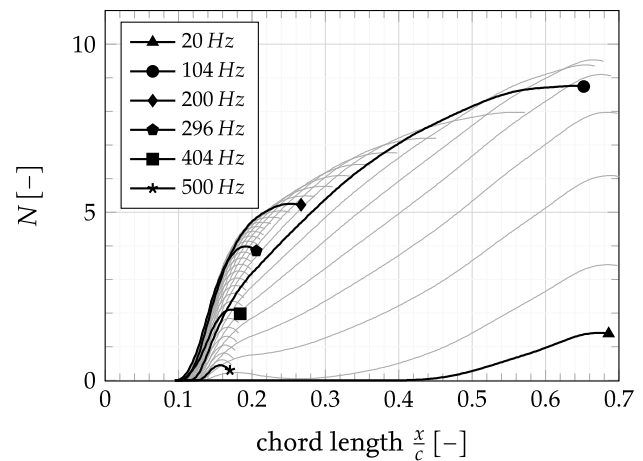


Fig. 8 Example of a N-factor envelope at $u_\infty = 10.64$ m/s and $Re = 1 \cdot 10^6$

distinguishes between the starting point of the transitional region:

$$N_{crit,1} \approx 2.13 - 6.18 \cdot \log_{10}(Tu) \tag{12}$$

and the end of the transitional region:

$$N_{crit,2} \approx 5 - 6.18 \cdot \log_{10}(Tu). \tag{13}$$

As can be seen, both formulas differ only in the leading constant summand. Combining this with the ideas of Narasimha (1957), then Eq. 12 is a correlation for \bar{x} and Eq. 13 is a correlation for $x(\gamma = 1)$. Hence, our definition of $x_{tr} := x(\gamma = 0.2)$ can be found with a simple linear interpolation to be:

$$N_{crit} \approx 2.704 - 6.18 \cdot \log_{10}(Tu) \tag{14}$$

In the experimental setup, the turbulence level Tu was determined from a single-sensor (single-wire) hotwire measurement in the freestream well outside any boundary layer, specifically at about $15 \cdot \delta$ above the plate surface. Each data acquisition ran for 10 s with a sample rate of 20 kHz. To avoid the influence of slow, low-frequency variations of the wind tunnel velocity, the measured velocity was high-pass-filtered with a cut-off frequency linearly varying with the tunnel velocity: 1 Hz at 4 m/s increasing to 5.2 Hz at 19 m/s. Then Tu was determined from the velocity fluctuations. The filter frequency is based on the notion that large-scale turbulence is limited by the fixed test section size.

Figure 9 shows the results of these freestream turbulence measurements. Tu decreases with increasing speed, which we found to be quite typical for wind tunnels with nozzles designed with the theory of Börger (1975). In any case, the quality of the wind tunnel seems suitable for studies of transitional flows.

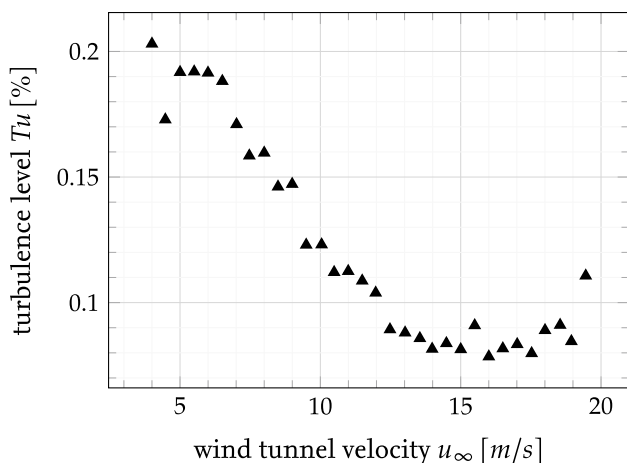


Fig. 9 Turbulence level measurements over the wind tunnel velocity

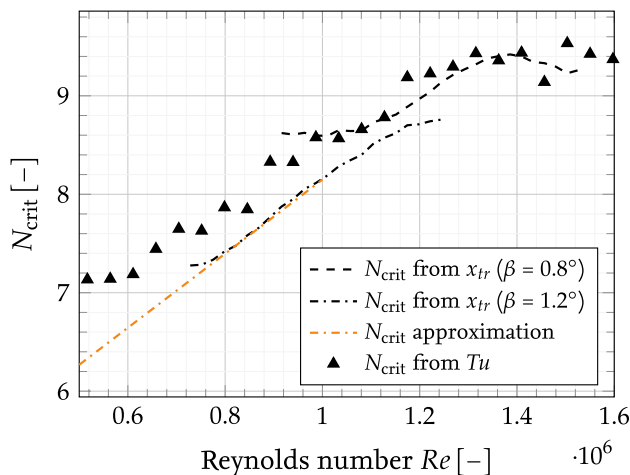


Fig. 10 Critical N-factors from turbulence level measurements and by direct measurement and the stability calculation

Applying the correlation Eq. 14 to the data shown in Fig. 9 gives an estimation of N_{crit} , which in Fig. 10 is compared with the direct determination of N_{crit} from the stability theory and the measured x_{tr} . As noted in Sect. 2.1, a direct measurement of N_{crit} from x_{tr} is only possible, if the (natural) transition is in the range of the microphones, which is the case for $0.8 \cdot 10^6 < Re < 1.2 \cdot 10^6$. However, for the ΔN methods a suitable N_{crit} is required for the whole velocity range of the wind tunnel. Therefore, to extent this range to larger Re a dataset with a smaller diffuser opening angle of $\beta = 0.8^\circ$ was used, assuming that the diffuser will not have a significant effect on N_{crit} itself. To extent the range to smaller Re , we pragmatically extended the measured curve with a linear approximation, which is also shown in Fig. 10. As can be seen from the figure, N_{crit} from Tu and that from x_{tr} were generally consistent in the setup. However, since the

correlation (14) to determine N_{crit} from Tu may be sensitive to the specific wind tunnel, the analysis of ΔN that will be shown in Sect. 3.2 is based on the three lines shown in Fig. 10.

Finally, Fig. 11 shows the development of the displacement thickness δ^* and the momentum loss thickness θ for the laminar boundary layer for one given flow case as an example, which is an immediate result of the boundary layer solution from COCO. The data are shown here for the sake of completeness, since the ΔN -models from Crouch et al. (2006), Perraud et al. (2014) and Hildebrand et al. (2020) are based on the relation of the step height h to the local boundary layer thicknesses, either δ^* or θ . Also shown is the resulting shape factor H_k . Since the flow features a weak adverse pressure gradient, the boundary layer is not a Blasius type, but at slightly higher $H_k \approx 2.75$. Nevertheless, the shape factor is rather constant over the relevant region $0.4 < x/c < 0.6$.

To allow a rebuilding of these cases, we also present the boundary layer profiles for a case with a step height of 1.5 mm and a Reynolds number of $Re = 7.1 \cdot 10^6$ in Fig. 12.

3 Results

3.1 Assessment of the step Reynolds number criterion

First, the general behavior of the intermittency for a backward-facing step with various step Reynolds numbers is shown in Fig. 13. The position of the step is shown by the dotted line at $x/c \approx 0.42$. The markers are the measured intermittency at the positions of the microphones, and the lines are the fitted curves based on (9) from Narasimha

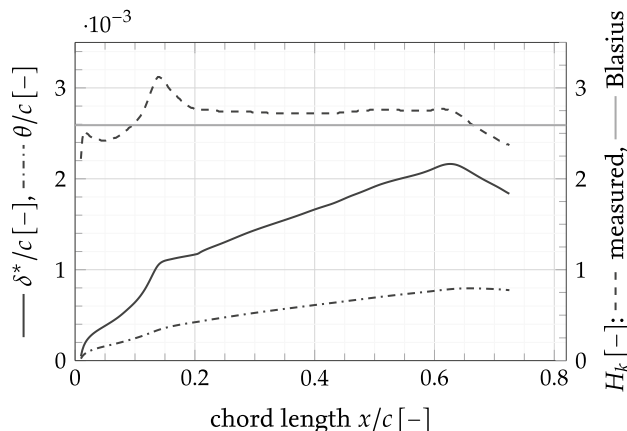


Fig. 11 Displacement and momentum thickness, δ^* and θ , and resulting shape factor H_k based on the experimental pressure distribution, at $u_\infty = 10.64 \text{ m/s}$, $Re = 10 \cdot 10^6$

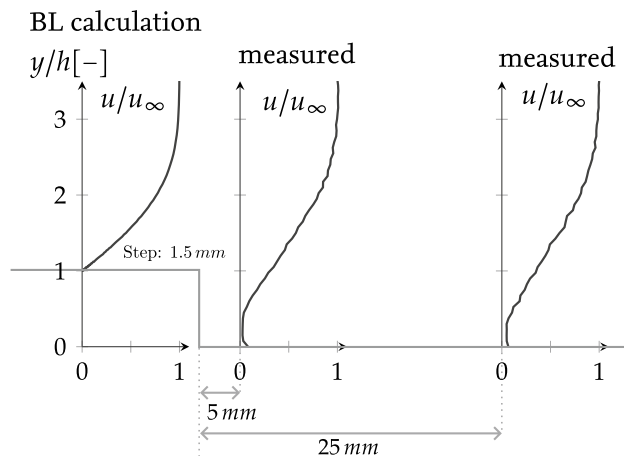


Fig. 12 Comparison of a calculated boundary layer from COCO shortly before and measured profiles 5 mm and 25 mm behind a 1.5 mm high step, at $u_\infty = 7.1$ m/s, $Re = 7.1 \cdot 10^6$

(1957). As can be seen, the fitted curves are generally a suitable representation of the measured data.

Two aspects are visible in Fig. 13: First, expectantly, transition is shifted upstream with increasing step Reynolds number. But also the length of the transitional region is becoming notably smaller with increasing step Reynolds number, i.e., transition to turbulence is happening more rapidly. Both aspects can be derived from the fitted curves, namely x_{tr} and λ .

Therefore, these two properties have been extracted for a larger number of cases and are shown in Fig. 14. For the transition position in Fig. 14a, it is still as expected that the transition is further upstream with increasing Re_h . The relevant critical step Reynolds number, ref. (2), is also shown. In the measured data, the critical step criterion is visible as a “kink,” i.e., the upstream shift of the transition position is becoming much weaker for critical and supercritical steps.

Note that herein we defined that $x_{tr} := x(\gamma = 0.2)$. Therefore, even for critical and supercritical steps, the transition position should always be some distance downstream of the step. In this case, for very large Re_h , the length of the transitional region becomes so small that the curve fitting is not very accurate, and therefore, the post-processing finally gives transition positions upstream of the step for large Re_h . This part of the data may not be physical, but the very supercritical steps are not of great interest anyway. Likely unphysical data with a transition position upstream of the step have therefore been grayed out in Figs. 14a and 16a.

The critical step Reynolds number can also be seen in the variation of λ in Fig. 14b: For subcritical cases, the transitional region is substantially larger than for critical or supercritical steps. It is actually the cases, as indicated by the line showing the length λ for the cases without any steps,

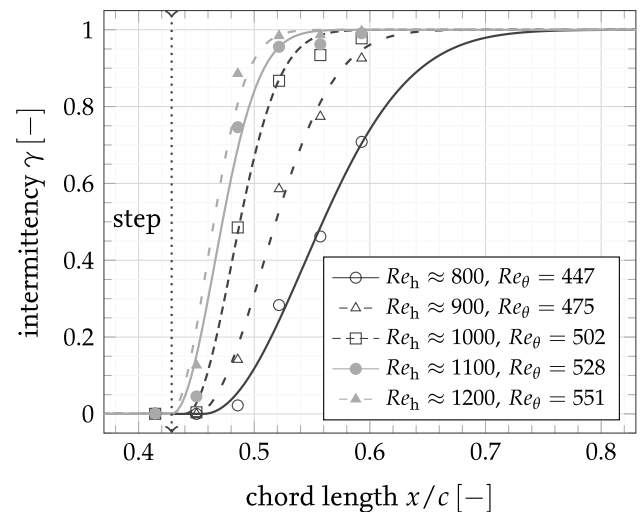


Fig. 13 Intermittency for a backward-facing step of 2 mm with different step Reynolds numbers

that subcritical steps create longer transitional regions than a natural transition process.

In summary, Fig 14 shows that for backward-facing steps the critical step height can be estimated from the critical step Reynolds number (2) with an acceptable accuracy. Critical and supercritical steps will lead to an initiation of the transition process and the length of the transitional region is smaller than for a natural transition, in this case around three times smaller.

Similar data, but for a forward-facing step, are shown in Figs. 15 and 16. Also for this case, the curves based on (9) are a good representation of the measured intermittency values. As for the backward-facing step, the transition position moves toward the step with an increasing step Reynolds number. An obvious difference, however, is the change in the transition length. For forward-facing steps, λ is fairly constant as long as the step is subcritical and is also of similar magnitude as for a free transition without any steps—if not slightly smaller. λ is only majorly affected if the steps become critical, which then also leads to a small λ , or a very quick transition, respectively.

In terms of the critical Reynolds number, the Re_h criterion (3) is only a rather rough estimation. While for the smaller step of 2 mm the criterion $Re_h \approx 1800$ is rather underestimating, for the larger step of 3 mm the same criterion overestimates the impact of the step. Other experiments have also shown that the critical Re_h for forward-facing steps is not very universal. For example, Schrauf (2018) has suggested critical values as high as $Re_h \approx 3600$. He hypothesized a significant influence of the pressure gradient and the test cases.

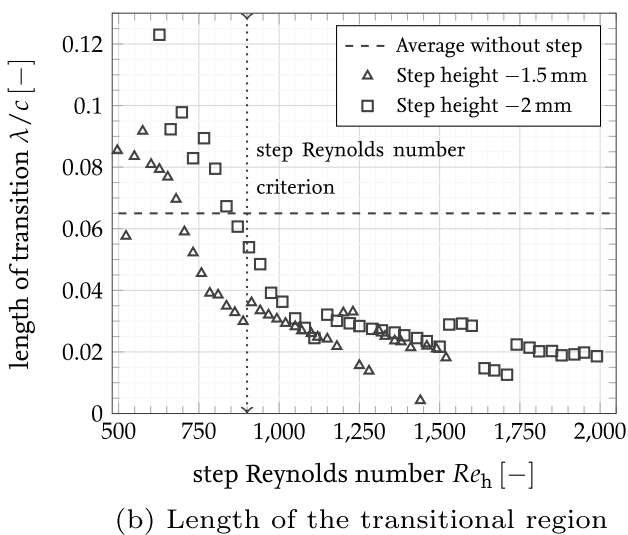
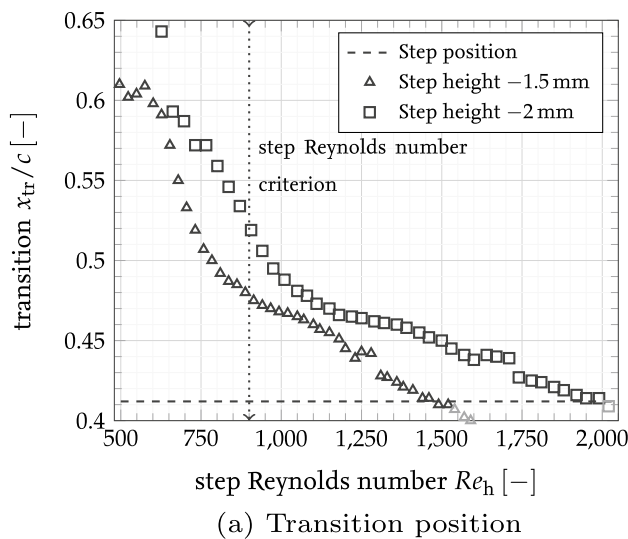


Fig. 14 Transition position and length of the transitional region for a backward-facing step with different step Reynolds numbers

3.2 ΔN of subcritical steps

As shown in Figs. 14 and 16, subcritical steps will usually not trigger transition right behind the step, but will still have an detrimental influence on the transition position and ΔN methods may be used to estimate this behavior, as explained in chapter 2.3.

The transition positions x_{tr} for all cases measured with a backward-facing step are shown in Fig. 17. Note that in this figure the axis of abscissa is *not* the step Reynolds number, but the chord Reynolds number of the flat plate. Still the influence of the step on transition can be seen and, again expectantly, large steps will shift transition upstream.

For further post-processing of ΔN, the N-factor envelope was determined by stability simulations akin to Fig. 8, based on the measured pressure distribution for the cases without

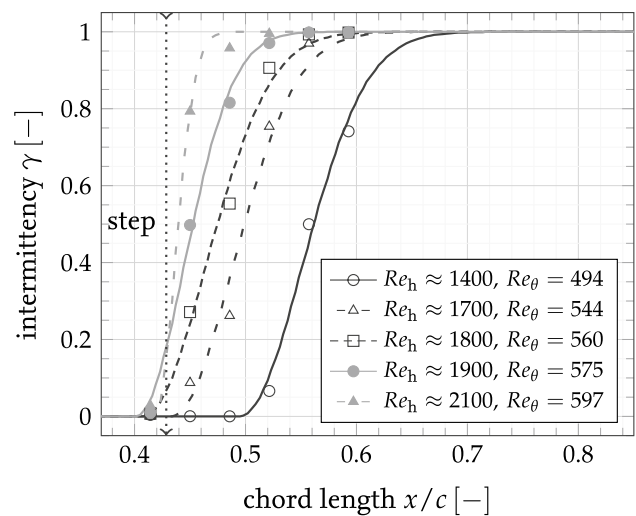


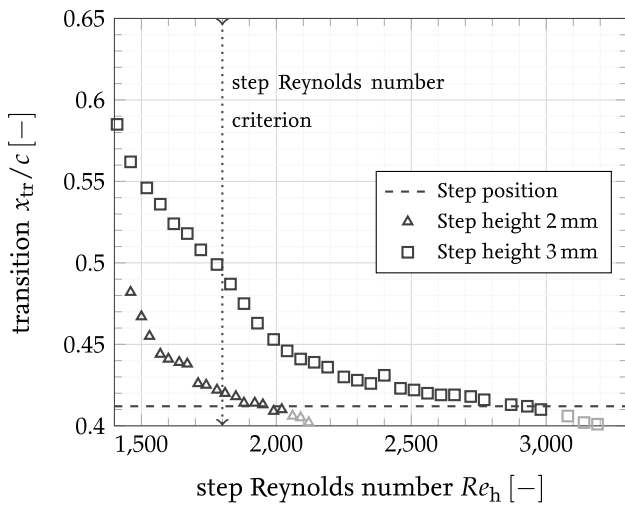
Fig. 15 Intermittency for a forward-facing step of 3 mm with different step Reynolds numbers

step, and the resulting N-factor at the transition position was subtracted from the critical N-factor shown in Fig. 10. These data are shown in Fig. 18, along with the respective models from Hildebrand et al. (2020) and Crouch et al. (2006) and the measurement data from Wang and Gaster (2005). The green markers represent critical or supercritical cases with $Re_h > 900$, which are generally expected not to correlate with any ΔN formulation. The black and orange markers are cases, where the criterion $Re_{h,BFS} < 900$ is met, i.e., subcritical cases. The black markers denote cases, where N_{crit} can be found by a direct measurement of x_{tr} without a step. As discussed in Fig. 10, for small wind tunnel velocities a linear approximation of N_{crit} was used and the cases that required this treatment are marked with orange markers.

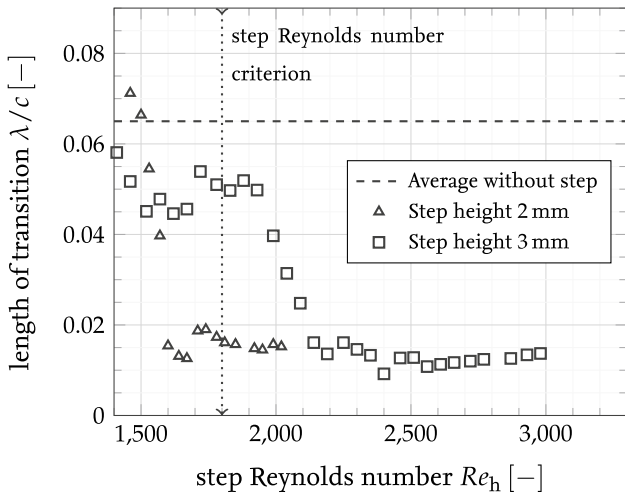
The resulting data points agree quite well with the theory from Hildebrand et al. (2020)—much better than with the linear estimation from Crouch et al. (2006). Supplementing this, we can further state that the measurement data of Wang and Gaster (2005) confirm this trend, especially for higher h/δ^* . We note, however, that the data from Crouch et al. (2006) are at much larger Reynolds numbers and also much larger ΔN, whereas the present setup is rather limited in maximum Re and also in maximum ΔN.

Obviously, the cases with green markers in Fig. 18 do not agree with neither one of the ΔN-estimations and, thus, show that a prior application of the critical Re_h criterion is required.

In Figs. 19 and 20, the data for the forward-facing steps are presented in a similar way. The transition positions for several different step heights in Fig. 19 show that, in contrast to the backward-facing steps, small forward-facing steps with $h < 1.5$ mm seem to have almost negligible influence on the transition position. Consequently, in Fig. 20 only the



(a) Transition position



(b) Length of the transitional region

Fig. 16 Transition position and the corresponding transition length for a forward-facing step plotted over the step Reynolds number

data for the two larger step heights are shown, since the steps with $h < 1.5$ mm are all $h/\delta^* < 0.4$ and effectively give $\Delta N \approx 0$. This small influence of small forward-facing steps on the N-factor can also be observed in DNS simulations, e.g., by Lüdeke and Soldenhoff (2021).

Consequently, the estimation (7), which passes through the origin, cannot describe this effect. It seems that for forward-facing steps, as based on our findings, some threshold value of h/δ^* is required, such that steps with $h/\delta^* < 0.4$ do not show any influence on the final transition position. Such minimum required step height is actually not evident in the data shown by Crouch et al. (2006) for neither adverse, nor favorable pressure gradient. This indicates that the relative step height h/δ^* cannot be the only parameter that determines ΔN for forward-facing steps. One conceivable reason

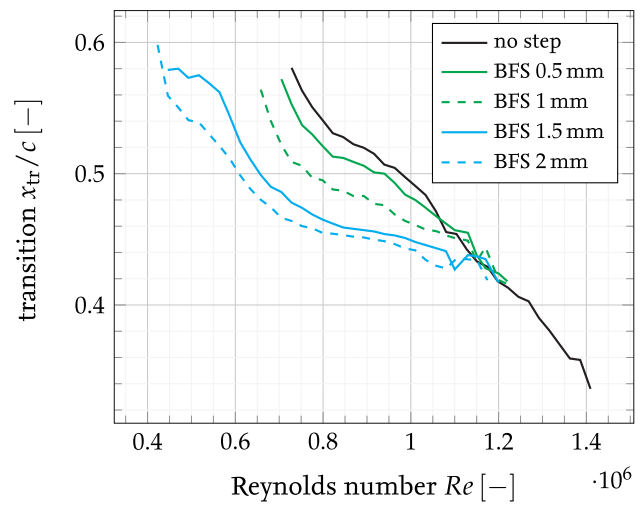


Fig. 17 Transition positions for backward-facing steps of different height

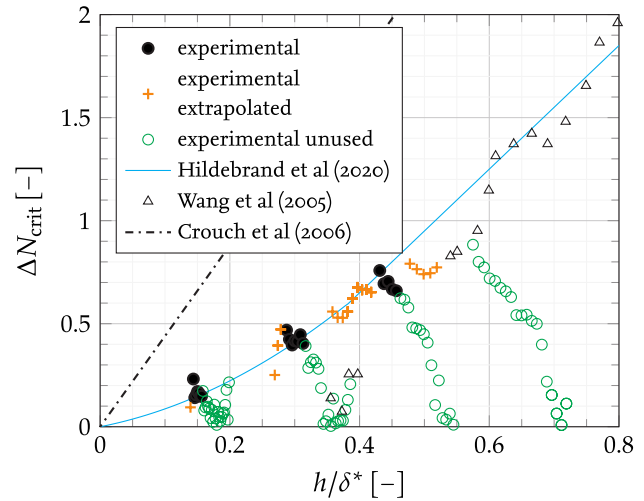


Fig. 18 Resulting ΔN for backward-facing steps compared with different models from the literature

could be, for example, that for small step heights the sudden, favorable pressure increase over the step actually stabilizes the flow, whereas for larger steps a separation bubble exists just behind the steps, which has a strong destabilizing effect. The influence of a separation bubble behind the step has been seen by Edelmann and Rist (2015) in numerical investigations.

We recall that also the critical Re_h for forward-facing steps, ref (3) and Fig. 16, seems to vary with the step height and is also obviously *not* an universal value. Both observations indicate that it may be required to sensitize, both, critical Re_h and ΔN models for forward-facing steps to some, yet unknown parameter to find more universal formulations.

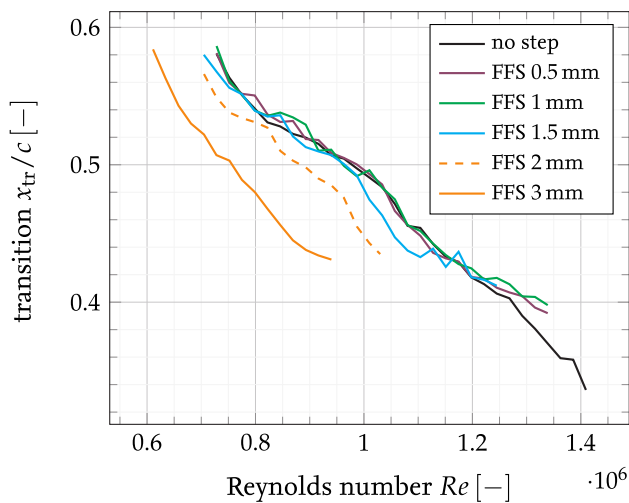


Fig. 19 Transition positions for forward-facing steps of different heights

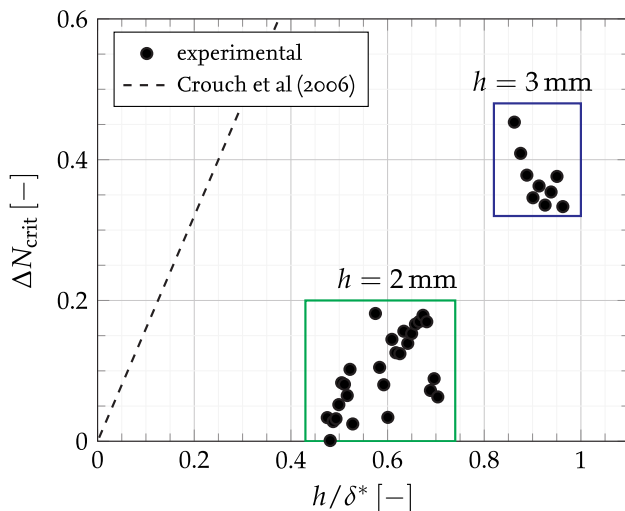


Fig. 20 Resulting ΔN for forward-facing steps compared with a model from the literature

4 Conclusion

The effects of steps on the transition of laminar boundary layers were measured on a flat plate in a small low-speed wind tunnel.

For backward-facing steps, the measured data could quite well confirm the concept of a critical step Reynolds number Re_h . Once Re_h is exceeded, transition is fixed near the step itself. For forward-facing steps, we also observed that, once the step is large enough, transition will be fixed near the step. However, the respective critical Re_h was not necessarily unique for different step heights.

The length of the transitional region, herein characterized as λ based on the intermittency data, changes substantially with the steps: For subcritical backward-facing steps, the transitional region was longer than for a natural transition. For subcritical forward-facing steps, the transitional region was not as long as for natural transition. For critical and supercritical steps, the transitional region was short, compared to any subcritical case or natural transition. Still, even in the case of a rather large, supercritical step, the transitional region covered several boundary layer thicknesses and a notable part of the chord. For our data, the intermittency data could well be approximated with the evolution proposed by Narasimha (1957).

For subcritical backward-facing steps, the new transition positions were consistent with the ΔN formulation of Hildebrand et al. (2020). For all the cases studied herein, all at low Reynolds number and rather low ΔN , this more recent approximation showed better agreement with the data than the linear relationships suggested by Crouch et al. (2006) or Perraud et al. (2014).

For subcritical forward-facing steps, the ΔN -approximation was not consistent with the formulation from Crouch et al. (2006) and our data seemed to follow a different trend, where small enough steps do not have any influence on the transition at all. Both the critical Re_h and the ΔN may be sensitive to some additional parameter yet not respected in the existing models. However, the presently existing data are not sufficient to really identify such parameter. From a technical point of view, the forward-facing steps are actually somewhat more interesting than the backward-facing ones, because given the same size of a step, they have less influence on the stability, or ΔN , respectively.

Acknowledgements The authors thank *DMT Druckmesstechnik GmbH* for providing additional pressure sensors and *Michelangelo Corelli Grappadelli* for providing a hotwire traverse system. We also acknowledge the support from *Dr. Camli Badrya*. We also acknowledge the Open Access funding from the University Library Braunschweig.

Author contributions AH and PS wrote the manuscript text. AH prepared all figures. All authors reviewed the manuscript.

Funding Open Access funding enabled and organized by Projekt DEAL. The work leading to these data has not received funding from other entities than the affiliations of the authors.

Availability of data and materials The used data can be provided by the authors on request.

Declarations

Conflict of interest The authors have no competing interests as defined by Springer Nature, or other interests that might be perceived to influence the results and/or discussion reported in this paper.

Ethical approval This declaration is not applicable.

Open Access This article is licensed under a Creative Commons Attribution 4.0 International License, which permits use, sharing, adaptation, distribution and reproduction in any medium or format, as long as you give appropriate credit to the original author(s) and the source, provide a link to the Creative Commons licence, and indicate if changes were made. The images or other third party material in this article are included in the article's Creative Commons licence, unless indicated otherwise in a credit line to the material. If material is not included in the article's Creative Commons licence and your intended use is not permitted by statutory regulation or exceeds the permitted use, you will need to obtain permission directly from the copyright holder. To view a copy of this licence, visit <http://creativecommons.org/licenses/by/4.0/>.

References

- Börger GG (1975) Optimierung von Windkanaldüsen für den Unterschallbereich. *Z Flugwiss* 23:45–50
- Crouch JD, Kosorygin VS, Ng LL (2006) Modeling the effects of steps on boundary-layer transition. Springer, Berlin. https://doi.org/10.1007/1-4020-4159-4_4
- Edelmann CA, Rist U (2015) Impact of forward-facing steps on laminar-turbulent transition in transonic flows. *AIAA J* 53(9):2504–2511. <https://doi.org/10.2514/1.J053529>
- Emmons HW (1951) The laminar-turbulent transition in a boundary layer-part i. *J Aeronaut Sci* 18(7):490–498. <https://doi.org/10.2514/8.2010>
- Eppler R (1990) Airfoil design and data. Springer, Berlin
- Fage A (1943) The smallest size of a spanwise surface corrugation which affects boundary-layer transition on an aerofoil. British Aeronautical Research Council Reports and Memoranda, pp 1–20. <https://reports.aerade.cranfield.ac.uk/bitstream/handle/1826.2/3987/arc-rm-2120.pdf?sequence=1>
- Grappadelli MC, Sattler S, Scholz P, et al (2021) Experimental investigations of boundary layer transition on a flat plate with suction. <https://doi.org/10.2514/6.2021-1452>
- Hildebrand N, Choudhari MM, Paredes P (2020) Predicting boundary-layer transition over backward-facing steps via linear stability analysis. *AIAA J* 58(9):3728–3734. <https://doi.org/10.2514/1.J059713>
- Krumbein A, Krimmelbein N, Schrauf G (2009) Automatic transition prediction in hybrid flow solver, part 2: practical application. *J Aircr* 46(4):1191–1199. <https://doi.org/10.2514/1.39738>
- Lüdeke H, Soldenhoff R (2021) Direct numerical simulation of TS-waves over suction panel steps from manufacturing tolerances. *CEAS Aeronaut J* 12(2):261–271. <https://doi.org/10.1007/s13272-021-00496-9>
- Mack LM (1975) A numerical method for the prediction of high-speed boundary-layer transition using linear theory. *Aerodyn Anal Requiring Adv Comput Part I*:101–123
- Narasimha R (1957) On the distribution of intermittency in the transition region of a boundary layer. *J Aeronaut Sci* 5(24):711–712
- Nenni J, Gluyas GL (1966) Aerodynamic design and analysis of an LFC surface. *Astronaut Aeronaut* 4(7):52
- Perraud J, Arnal D, Kuehn W (2014) Laminar-turbulent transition prediction in the presence of surface imperfections. *Int J Eng Syst Model Simul* 6(3/4):162–170. <https://doi.org/10.1504/IJESMS.2014.063129>
- Schiller L (ed) (1932) Rohre, offene Gerinne, Zähigkeit, Handbuch der Experimentalphysik, vol 4, 1st edn. Akademische Verlagsgesellschaft M.B.H, Leipzig
- Schrauf G (1998) COCO-A program to compute velocity and temperature profiles for local and nonlocal stability analysis of compressible, conical boundary layers with suction. ZARM Technik report 780
- Schrauf G (2006) LILO 2.1: user's Guide and Tutorial. Technical report, Deutsches Zentrum für Luft- und Raumfahrt e.V., Bremen
- Schrauf G (2018) On allowable step heights: lessons learned from the F100 and ATTAS flight tests. In: 6th European conference on computational mechanics (ECCM 6), Glasgow, p 12
- Schubauer GB, Klebanoff PS (1955) Contributions on the mechanics of boundary-layer transition. NACA TN 3489 <https://ntrs.nasa.gov/api/citations/19930092285/downloads/19930092285.pdf>
- Smith A, Clutter D (1959) The smallest height of roughness capable of affecting boundary-layer transition. *J Aerosp Sci* 26(4):229–245
- Smith A, Gamberoni N (1956) Transition, pressure gradient and stability theory. Douglas aircraft report no. ES 26388
- Tani I, Hama FR (1953) Some experiments on the effect of a single roughness element on boundary-layer transition. *J Aeronaut Sci* 20(4):289–290. <https://doi.org/10.2514/8.2613>
- van Ingen JL (1956) A suggested semi-empirical method for the calculation of the boundary layer transition region. Technische Hogeschool Delft, Vliegtuigbouwkunde, Rapport VTH-74 <https://repository.tudelft.nl/islandora/object/uuid>
- van Ingen JL (2008) The en method for transition prediction. historical review of work at tu delft. In: Proceedings of the 38th AIAA fluid dynamics conference and exhibit, Seattle, Washington, pp 1–49. <https://doi.org/10.2514/6.2008-3830>
- Wang YX, Gaster M (2005) Effect of surface steps on boundary layer transition. *Exp Fluids* 39(4):679–686. <https://doi.org/10.1007/s00348-005-1011-7>
- Wie YS, Malik MR (1998) Effect of surface waviness on boundary-layer transition in two-dimensional flow. *Comput Fluids* 27(2):157–181. [https://doi.org/10.1016/S0045-7930\(97\)00024-8](https://doi.org/10.1016/S0045-7930(97)00024-8)

Publisher's Note Springer Nature remains neutral with regard to jurisdictional claims in published maps and institutional affiliations.